MURAJ
Minnesota Undergraduate Research & Academic Journal

z.umn.edu/MURAJ

Structural and Transport Characterization of Ti and $La_{0.7}Sr_{0.3}Mn_{O3}$ Thin Films to become Non-Local Spin Valves

Emma Bernard

Abstract

Structural and transport characterization of thin films is important for the fabrication and performance of non-local spin valves, NLSVs, especially when new materials are integrated into the device. In the present study, thin films of one non-magnetic metal, Ti, and one ferromagnetic oxide, La0.7Sr0.3MnO3 (LSMO), were characterized to illustrate the general process of preparing and analyzing thin films for NLSVs. NLSVs allow for the material properties of spin polarization and spin diffusion length to be measured. These properties have applications in expanding the efficiency of spintronic devices. For structural characterization, the thickness of each thin film was measured using x-ray reflectometry. For transport characterization, the resistance of each thin film was measured over a range of temperatures. The resistance of the thin film was related to resistivity using the Van der Pauw equation. The relationship between resistivity and temperature provides insight into the purity of the thin film through the residual resistivity ratio, RRR, and the Curie temperature, Tc, (for ferromagnetic materials). A comparison of the properties of fabricated LSMO nanowires to their starting films show a similar Tc and RRR, suggesting that the quality of the material was not compromised during the fabrication process.

Introduction

The advent of spintronic devices and spin valve technology has allowed for the development of devices used to read and store data industrially, such as magnetic sensors, hard disk read heads, and magnetic random-access memory [1]. Spintronics allow for the electron's spin degree of freedom to be utilized in addition to electrical current [2]. Spin is incorporated into devices using ferromagnetic (FM) materials because current passing through the FM becomes polarized [3]. A FM's ability to polarize a current is known as spin polarization, α, which is defined as the difference in conductivity between the spin up and spin down states divided by the total spin conductivity [4]. A typical spin valve, such as current-perpendicular-to-plane spin valve (CPP) seen in Figure 1(a), consists of two FM layers, conventionally Fe or Co, that sandwich a variety of spacer materials: non-magnetic (NM) metals like Al or Cu, tunnel barriers, semiconductors, or semimetals [5]. NM are typically chosen based on the distance before a non-equilibrium spin current changes sign, also known as spin diffusion length, λ [6].

As new materials are integrated into

CC BY NC

CPPs, non-local spin valve devices, NLSVs, are designed to measure the properties fundamental to the function of CPPs, such as λ [6]. In contrast to a CPP in which the NM is sandwiched in between the two FMs, NLSVs are "non-local" due to the separation, *d,* of the two FMs perpendicular to the NM. A typical NLSV is shown schematically in Figure 1(b). The goal of NLSVs is to isolate a pure spin current on a NM conducting nanowire between two laterally aligned FM electrodes [5]. This is possible due to the non-local location of the detector, FM^1, and injector, FM^2, electrodes [5]. When an electrical current is flown through FM^1, the current becomes polarized and is injected into the NM, driven by a potential, *V*, to FM^2 [5]. As the polarized spin diffuses through NM and nonequilibrium spin accumulates at the boundary of NM and FM^2, *V* spontaneously drops creating a signal [5]. The relative sign of *V* indicates the magnetic configuration, parallel or anti-parallel, of the two FM electrodes [7]. The magnetization of the detector and injector FMs depends on the applied magnetic field, *H* [5].

By picking a FM material that enhances *α*, and a NM material that enhances λ, the transport properties of the device can be controlled and the efficiency of spin injection can be improved, resulting in a larger voltage signal [6, 3]. The NLSV signal can also be represented as a change in resistance, R, between the parallel and anti-parallel states, defined as the nonlocal resistance, RNL [7, 4]. The R_{NL} is a function of device dimensions, *d*, and is expressed by,

$$\Delta R_{NL} = 4\frac{\alpha^2 R_{FM}^2}{(1-\alpha^2)^2 R_{NM}} \frac{exp\left\{-\frac{d}{\lambda_{NM}}\right\}}{\left[1+\frac{2R_{FM}}{(1-\alpha^2)\ \ R_{NM}}\right]^2 - exp\left\{-\frac{2d}{\lambda_{NM}}\right\}} \qquad (1)$$

where R_{FM} is the resistance of the FM, R_{NM} is the resistance of the NM, λ_{NM} is the spin diffusion length of the NM, and α is the polarized spin current of the FM, as previously defined [4]. The larger the α, the larger the R_{NL}, and thus, the larger the signal. Since NLSVs separate charge and spin current, λ_{NM} can be measured making NLSVs a powerful tool for measuring spin transport properties in NM materials [5]. Equation 1 highlights the importance of characterizing the structural and transport properties of the NLSV FM and NM starting materials.

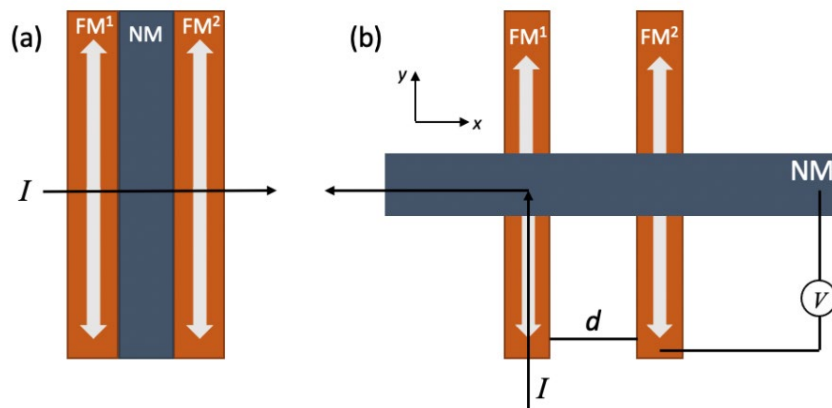

Figure 1 A schematic of (a) a CPP spin valve where FM^1 and FM^2 have different coercivities and (b) a NLSV where FM^1 is the injector and FM^2 is the detector. For NLSVs, an electrical current, *I,* is run through FM^1 and the voltage, *V*, is measured at the NM wire and FM^2 a distance, *d,* away from FM^1. Given an applied magnetic field, the white arrows indicate the relative FM magnetization state between parallel and anti-parallel configurations [5].

Initial material selection and characterization is important for designing and preparing NLSVs because geometry, transport properties, and magnetic properties impact device functionality. Typically, NLSVs are made out of FM/NM metals. However, new research has focused on developing oxides to be either the FM electrodes or NM wires due to their enhanced degrees of freedom which allow for various physical properties to be tuned for a specific function [2]. One example of an FM oxide being studied is $La_{0.7}Sr_{0.3}MnO_3$, LSMO, due to its theoretical 100% spin polarization which maximizes the R_{NL} obtained from Equation 1 [8]. On the other hand, titanium, Ti, is being studied as a potential NM metal due to its theoretically large λ_{NM} based on its low atomic number and spin-orbit coupling [9].

Before NLSVs are made, the transport properties of the fabricated nanowires and their starting thin film are compared in order to evaluate if the quality of the material is maintained during fabrication. Quality is quantified by the residual resistivity ratio, RRR, and the similarity in the magnetoresistance, MR, to the Curie temperature, T_C [10]. Specifically, MR is the change in resistance of a FM caused by a magnetic field, where an absolute maximum near T_C is attributed to the switching of magnetic polarons, an electron transport property, near the paramagnetic and ferromagnetic transition [10]. Fabrication of LSMO is especially difficult because the epitaxial thin film is susceptible to damage where any defects introduced through the fabrication process can lower the quality of the material, and thus its performance as a NLSV.

This paper will focus on preparing LSMO and Ti to become NLSVs based on the structural characterization and transport measurements of characterization and transport measurements of their thin films. Structural characterization of the thin films consists of measuring x-ray reflectometry, XRR. Transport characterization involves the measurement of R across multiple temperatures, *T*, and magnetic fields, *H*. Once the thin film is characterized, the results are compared to those of nanowires fabricated from their respective thin film. Relevant literature values of the characterized materials and their substrates are included in Table 1.

Experimental

LSMO epitaxial films were grown in a Jülich Research high-oxygen pressure oxide

Table 1 A summary of materials to be characterized, literature value of mass density, ρd, and bulk Van der Pauw (vdP) resistivities ρRT,VDP, at room temperature (RT). The Miller index plane (001) was used for both **substrates**

Material	Function	$\rho_{RT,VDP}$ (mΩcm)	ρ_d (g/cm^3)	Reference
$La_{1-x}Sr_xMnO_3$ (x=0.3) (LSMO)	FM	1-2	6.5	[10]
$(LaAlO_3)_{0.3}(Sr_2TaAlO_6)_{0.7}$ (LSAT (001))	substrate	--	6.65	[11]
Titanium (Ti)	NM	0.042	4.51	[12]
Silicon (001) (Si (001))	substrate	--	2.33	[13]

sputtering system on (001) LSAT. Ti was grown with molecular beam epitaxy, MBE, on (001) Si. For all thin films, XRR was performed using the Rigaku SmartLabXE to measure film thickness with Cu-Kα X-rays with a wavelength, $\lambda_{Cu\text{-}K\alpha}$, of 1.54 Å. For both metals and oxide films, the scan was completed from 0.2° to 5° with a step size of 0.1° at 0.24°/minute.

A Quantum Design Physical Properties Measurement System, PPMS, was used to complete temperature sweeps from 5 K to 400 K (or 300 K for Ti) while measuring changing resistance at either 0 T or 9 T magnetic fields. A current verses resistance measurement was completed before measuring a resistance verses temperature in order to find a suitable current that shows ohmic behavior.

Results and Discussion

The performance of NLSVs are impacted by geometry and electron transport properties. Therefore, the structural and transport properties of a thin film of each material are characterized before NLSVs are grown. For a given thickness, *t*, the thin film can be compared to its nanowire counterpart to evaluate changes in transport properties and ensure successful device fabrication.

Two methods of analyzing XRR data for *t* are commonly used. Figure 2 compares these methods for the Ti and LSMO thin films. The XRR output can be plotted as reflectivity with units of absolute unit, a.u, as in Figure 2(a) and Figure 2(c), or as intensity with units of counts, cps, as shown in Figure 2(b) and Figure 2(d).

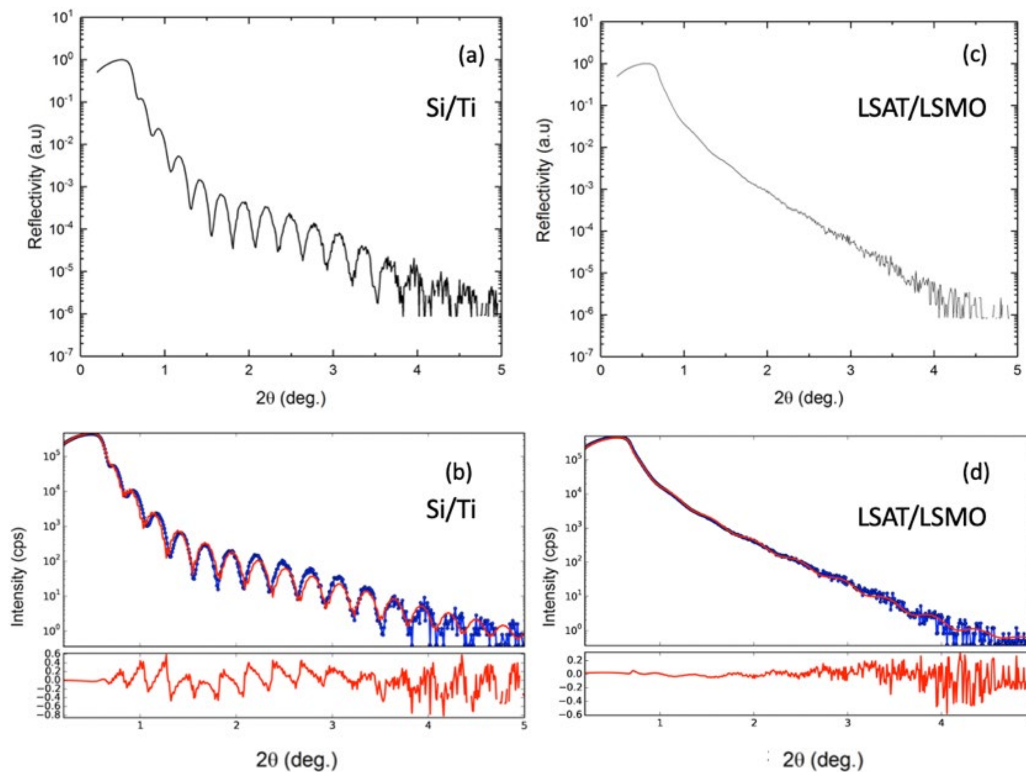

Figure 2 For the (a) XRR absolute reflectivity and (b) GenX fitting of a Ti thin film, the Kiessig equation yielded a thickness of 31.13 nm and GenX fitting yielded a thickness of 30.63 nm, respectively. For the (c) XRR absolute reflectivity and (d) GenX fitting of a LSMO thin film, the Kiessig equation yielded a thickness of 15.05 nm GenX fitting yielded a thickness of 17.7 nm, respectively. Intensity is converted into absolute reflectivity in Appendix A.

The distinction between reflectivity and intensity is explained in Appendix A. In both cases, the data can be analyzed to find *t*. The first fitting method is GenX which uses the Parratt recursion formula and material property inputs to fit XRR outputs [14]. The Parratt recursion formula states that the shape of the curve can be predicted based on the particle model and properties of the film, such as electron density, assuming that there is a sharp distinction between the film and substrate [15]. The particle model is shifted such that the theoretical and experimental curves align more closely, and the film thickness is determined [15]. Alternatively, the Kiessig equation uses fringe pattern spacing in the XRR output to extract *t*. The Kiessig Equation states,

$$sin^2(\theta_{N+k}) = \left[\frac{(N+k)\lambda_{Cu}}{2t}\right]^2 + 2\delta \quad (2)$$

where $\theta_{(N+k)}$ is the angle where the local maxima occur, *N* is the order index integer of the fringe maxima, and δ is a material property (based on the index of refraction) used to calculate the transition between total external reflection of the x-rays and the beginning of refraction (see Appendix A) [16]. Alternatively, local minima can also be observed for $\theta_{(N+k)}$ and *N,* in order to determine which calculated *t* has the highest linearity, as shown in Appendix A. In general, the spacing of the fringes can be used to determine *t* based on the interference of reflected x-rays at the surface with the refracted x-rays between film and substrate [16]. Higher frequency of oscillations results in shorter periods, and thus a thicker film. A low noise to signal ratio indicates low surface roughness [16]. Additionally, the large fringe amplitude is characteristic of a film with a large difference in mass density, ρ_d, from its substrate; one example being the Ti thin film and (001) Si substrate as shown in Figure 2(a) (ρ_d reported in Table 1) [16]. For comparison, as seen in Figure 2(c), the peaks for the LSMO film are smaller due to its similarity in density to the LSAT substrate. The LSMO thin film has a measured *t* of 17.7 nm. Using the measured *t*, transport measurements can be normalized into transport properties.

Both the LSMO and Ti thin films were characterized for their transport properties using the PPMS R v T sweep at 0T. LSMO had an

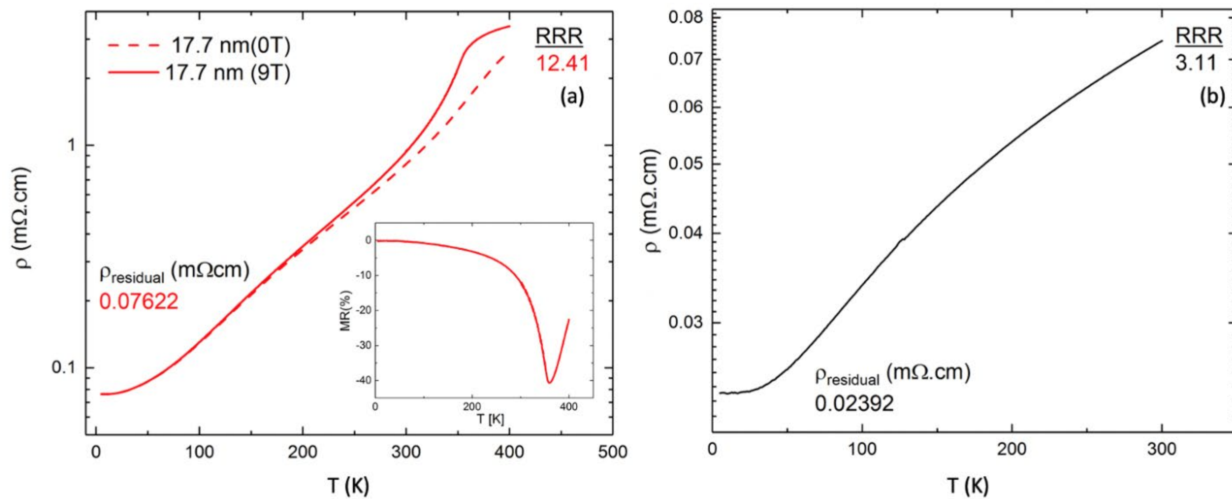

Figure 3 The (a) log (ρVDP) v T for the LSMO thin film from 0K to 400K at 0T and 9T and (b) log (ρVDP) v T for the Ti thin film from 0K to 300K at 0T. The inset in (a) shows %MR for the LSMO film of thickness 17.7 nm with a minimum at 359 K.

Both the LSMO and Ti thin films were characterized for their transport properties using the PPMS *R v T* sweep at 0T. LSMO had an added sweep at 9T. Each measured *R* is related to resistivity, p_{VDP}, using the determined *t* and the Van der Pauw, vdP, equation, where R_1 and R_2

$$\rho_{VDP} = \frac{\pi t}{\ln(2)}\left(\frac{R_1+R_2}{2}\right) f\left(\frac{R_2}{R_1}\right) \quad (3)$$

are the average measured 4-terminal resistances in the *x* and *y* directions [17]. See Appendix B for a more detailed description of the Van der Pauw equation. For a range of *T*, p_{VDP} is calculated and plotted in Figure 3 for both Ti and LSMO. Manifested in various ways, p_{VDP} vs *T* can be used to analyze RRR, dρ/dT, and the %MR (if the sweep is completed at multiple *H*), calculated in Appendix B [10]. As seen in the Figure 3(a), the peak for the LSMO film is at 359 K which is approximately equal to the T_C for bulk LSMO, 360 K [3, 7]. The peak of %MR is often compared to the peak of dρ/dT at 0T, which also occurs near T_C (Appendix B). Lower T_C can be linked to lower LSMO film quality [10]. Thin film quality can further be expressed by the residual resistivity ratio, RRR, using the change in pVDP from 0K to 300K, also calculated in Appendix B [18]. For LSMO the RRR was calculated to be 12.41. However, for LSMO, the changing T_C with sample purity must be considered because as T_C is nearly 300K, shifts in T_C will greatly impact the ρ_{300K} and thus the RRR.

As a NM metal, the purity of the Ti film is related more to RRR than %MR because Ti is paramagnetic so *R v T* at 9T was not measured [19]. At low temperatures, p_{5K} depends on impurities and defects, while at high temperatures, p_{300K} depends on lattice vibrations [19]. The RRR captures the quality of the film in this way and was calculated to be 3.11 for Ti. It is the function of the NM to transport the spin polarized current from the injector electrode to the detector electrode, so transport properties of the NM are paramount in calculating the spin diffusion length, λ, as described by Equation 1.

Once a NLSV is designed, the resistivity of the FM, ρ_{FM}, cannot be measured. For this reason, freestanding nanowires were fabricated to evaluate if the properties of the nanowires were comparable to those of the starting film, thus indicating a successful fabrication[1]. A nanowire was fabricated from the 17.7 nm LSMO film with a length, *l*, of 3000 nm and a nominal width, *w*, of 160 nm. The

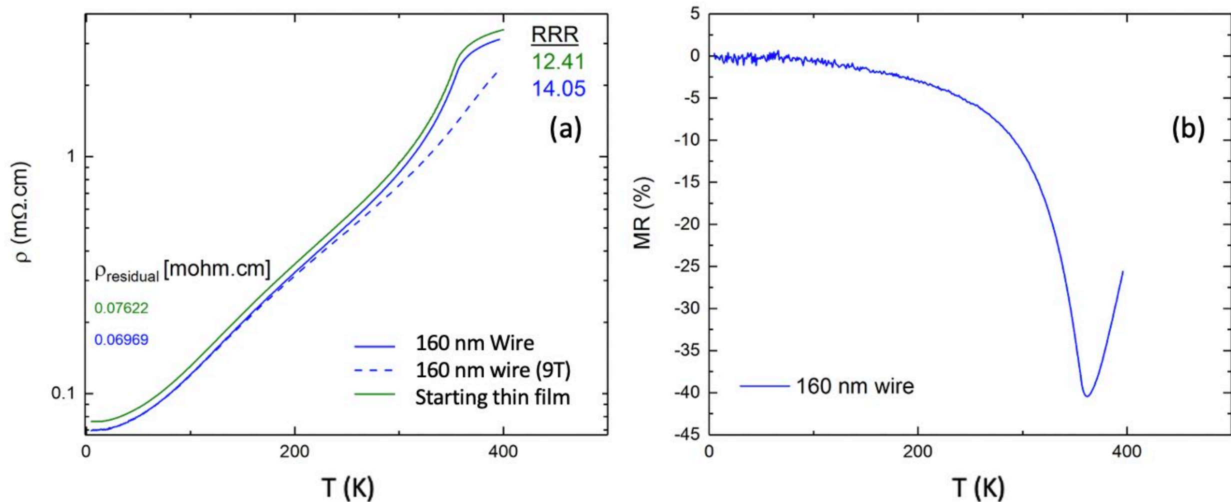

Figure 4 (a) The log(ρ_{VDP}) v T from 0K to 400K at 0T and 9T and (b) the %MR of the 160 nm wide LSMO nanowire and the starting 17.7 nm film. The %MR minimum occurs at 361.06 K.

thickness, t, is the same as that of the starting film, 17.7 nm. A R vs T sweep was completed at both 0T and 9T, as shown in Figure 4. The results of the starting 17.7 nm thin film are also included in Figure 4 to show the similarity in ρ vs T between the nanowires and the thin film. The vdP equation cannot be applied to the calculation of ρ for the nanowires. Instead, ρ is calculated from,

$$\rho = \frac{R*t*w}{l} \tag{4}$$

where R is measured from a 4-contact wire configuration [12]. It is possible for the fabrication process to damage the crystal structure and change the properties of the thin film, hence the agreement in values for the RRR and %MR peak of the thin film with the nanowire indicates a successful fabrication of the LSMO film. Calculated in Appendix B, the RRR of the nanowire had a percent difference of 13.32% to the RRR of the starting thin film, and the %MR of the nanowire and starting thin film was 0.5738% different. These results suggest a similar fabrication process should be used to create the NLSV. A similar experiment could be performed for the Ti films.

Conclusion

Ti and LSMO are examples of new materials being studied for NLSV applications—Ti for NM and LSMO for FM—however many transition metals and oxides alike are being characterized in a similar manner to be fabricated into NLSV. Ti is of interest because once a NLSV is fabricated, the spin diffusion length, λ_{NM}, can be calculated from further R_{NL} experimentation, using the well-characterized structure and transport properties of its thin film. LSMO is another class of material with potential in magnetoelectronic devices due to the high spin polarization, α. As demonstrated by the similarity in the properties of the LSMO nanowire with its respective thin film, the success of NLSV fabrication can be predicted based on structural and transport characterization. Specifically, the RRR of the nanowire had a percent difference of 13.32% to the RRR of the starting thin film, and the minimum %MR of the nanowire was 0.5738% different than the minimum %MR of the starting thin film. Thus, a successful development and characterization of both a NM and FM thin film is discussed.

[1]The nanowires were prepared by e-beam lithography and argon ion milling, using a negative resist mill mask. Prior to milling, Mg (5 nm) / Au (100+ nm) contacts were deposited by e-beam lithography and DC sputtering.

Acknowledgements

I would like to thank Chris Leighton for advising this project and John Dewey, Justin Ramberger, and Ben Kaiser for training me on experimental techniques/analysis as well as providing constructive feedback.

References

[1] “Introduction to Spintronics and Spin Quantum Computation,” *University of Maryland*. [Online]. Available: https://www.physics.umd.edu/rgroups/spin/intro.html.

[2] M. Bibes and A. Barthélémy, “Oxide spintronics,” *IEEE Trans. Electron Devices*, vol. 54, no. 5, pp. 1003–1023, 2007, doi: 10.1109/TED.2007.894366.

[3] M. Bowen, *Spintronics: An application of complex metal oxides. An application of complex metal oxides.* Elsevier Ltd, 2015.

[4] L. O’Brien *et al.*, “Kondo physics in non-local metallic spin transport devices,” *Nat. Commun.*, vol. 5, no. May, 2014, doi: 10.1038/ncomms4927.

[5] J. D. Watts, “Spin Relaxation and Size Effects in Cu and Al Nanowires,” no. December, 2018.

[6] J. Bass and W. P. Pratt, “Spin-diffusion lengths in metals and alloys, and spin-flipping at metal/metal interfaces: An experimentalist’s critical review,” *J. Phys. Condens. Matter*, vol. 19, no. 18, 2007, doi: 10.1088/0953-8984/19/18/183201.

[7] Y. Otani and T. Kimura, “Manipulation of spin currents in metallic systems,” *Philos. Trans. R. Soc. A Math. Phys. Eng. Sci.*, vol. 369, no. 1948, pp. 3136–3149, 2011, doi: 10.1098/rsta.2011.0010.

[8] I. I. Mazin *et al.*, “Origin of high transport spin polarization in La0.7Sr0.3MnO3: Direct evidence for minority spin states,” *Phys. Rev. B - Condens. Matter Mater. Phys.*, vol. 63, no. 18, pp. 1844331–1844335, 2001, doi: 10.1103/physrevb.63.184433.

[9] Y. Niimi, D. Wei, H. Idzuchi, T. Wakamura, T. Kato, and Y. Otani, “Experimental verification of comparability between spin-orbit and spin-diffusion lengths,” *Phys. Rev. Lett.*, vol. 110, no. 1, pp. 1–5, 2013, doi: 10.1103/PhysRevLett.110.016805.

[10] Y. Wenhao *et al.*, “Highly orientated growth and characterization of La0.7Sr0.3MnO3 thin films with different orientations on SrTiO3 substrates by chemical solution deposition method,” *J. Appl. Phys.*, vol. 117, no. 17, pp. 3–7, 2015, doi: 10.1063/1.4906947.

[11] Pierre Villars, “(LaAlO3)0.3(Sr2AlTaO6)0.35 substrate (Sr0.7La0.3Ta0.35Al0.65O3) Crystal Structure,” *Springer Materials*, 2016. [Online]. Available: https://materials.springer.com/isp/crystallographic/docs/sd_1924019.

[12] W. D. Callister, *Materials Science and Engineering: An Introduction*, 9th ed. 2014.

[13] B. M. Askerov, “Silicon,” *World Scientific*, 1994. [Online]. Available: http://lampx.tugraz.at/~hadley/memm/materials/silicon/silicon.php#:~:text=The density of silicon is,is 4.99 × 1028.

[14] M. Björck and G. Andersson, “GenX: An extensible X-ray reflectivity refinement program utilizing differential evolution,” *J. Appl. Crystallogr.*, vol. 40, no. 6, pp. 1174–1178, 2007, doi: 10.1107/S0021889807045086.

[15] L. G. Parratt, “Surface studies of solids by total reflection of x-rays,” *Phys. Rev.*, vol. 95, no. 2, pp. 359–369, 1954, doi: 10.1103/PhysRev.95.359.

[16] H. Steinrück, “X-ray Surface Diffraction Reflectivity,” *Stanford Synchrotron Radiat. Light. SLAC Natl. Accel. Lab.*, 2016.

[17] L. J. Van Der PAUW, “A method of measuring the resistivity and Hall coefficient on lamellae of arbitrary shape,” *Philips Technical Review*, vol. 20, no. 8. pp. 220–224, 1958.

[18] Charels Kittel, *Introduction to Solid State Physics*, 8th ed. John Wiley & Sons, Inc, 2005.

[19] F. R. Ficket, “Electrical Properties of Materials and Their Measurment at Low Temperatures,” *NBS Tech. Note*, 1982.

Appendices

Appendix A: Structural Characterization of Thin Films

The Kiessig Equation, shown in Equation 2, can be linearized as,

$$m = \frac{sin^2(\theta_{N+k})}{N^2} = \frac{\lambda^2}{4t^2} \quad \text{(A1)}$$

to solve for the thickness of the film. $\theta_{(N+k)}$ is the angle where the local maxima or minima occur, *N* is the order index integer of the fringe maxima or minma, λ is the wavelength of Cu-Kα x-rays, 1.54 Å, and *t* is the thickness [16]. Both local maximum and local minimum, $\theta_{(N+k)}$, are chosen to determine the resulting *t* with the highest linearity. The first index integer, N_o, is 1 for local minima and 2 for local maxima. For example, local minima yielded the lowest correlation (1-R) for the Ti thin film for the thickness of 31.13 nm.

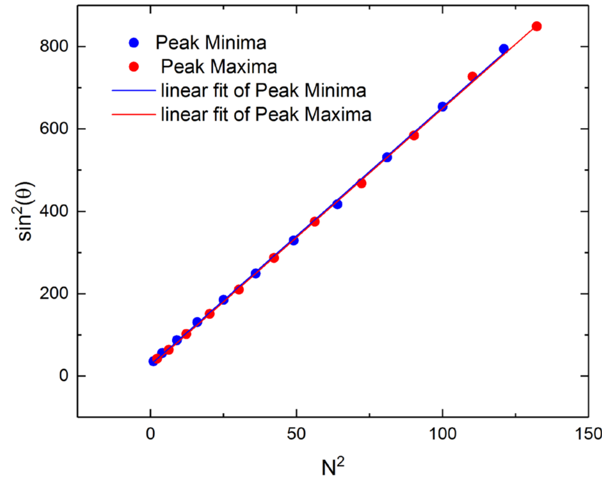

Figure A1 The linearization of fringe peak minima and maxima for a Ti thin film. For fringe peak minima, the slope is 6.18 with a correlation (1-R) of 0.0167. The thickness is 31.02 nm. For fringe peak maxima, the slope is 6.13 with a correlation (1-R) of 0.007. The thickness is 31.13 nm.

Plots of measured intensity, *I,* can be converted into reflectivity, R_I, using the equation

$$R_I = \frac{I}{I_o} \quad \text{(A2)}$$

where I_o is the maximum intensity. The change in *y*-axis for the plot of Ti on (001) Si can be observed in Figure A2.

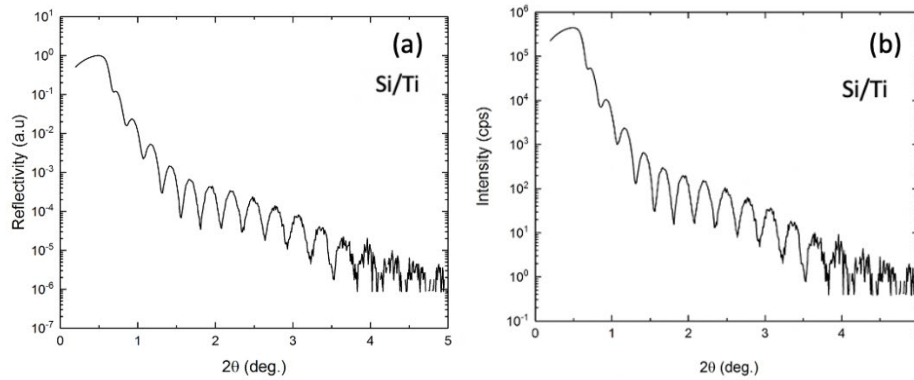

Figure A2 A comparison of plotting (a) absolute reflectivity vs 2θ to (b) intensity vs 2θ.

Appendix B: Calculating Van der Pauw Resistivity

Van der Pauw, vdP, resistivity is a method for measuring the resistance in an arbitrarily shaped thin film. The general form is,

$$\rho_{VDP} = \frac{\pi d}{\ln(2)}\left(\frac{R_1+R_2}{2}\right) f\left(\frac{R_2}{R_1}\right) \quad \text{(B1)}$$

where R_1 and R_2 are the average measured 4 terminal resistances, d is the thickness of the sample, and ρ_{VDP} is the final resistivity per temperature [17]. Figure B1 shows how R_1 and R_2 are measured schematically. Electrical contacts are placed at location *A, B, C,* and *D* on the thin film. From an applied voltage, *V*, and current, *I*, two resistances can be measured from the two different configurations, shown as R_1 and R_2 in Figure B1. Together, R_1 and R_2 are related to the ρ_{VDP}, as shown in Equation B1. It is assumed that the material is isotropic, and that the electrical contacts are small compared to the size of the sample, thus not impacting the resistance reading, [17].

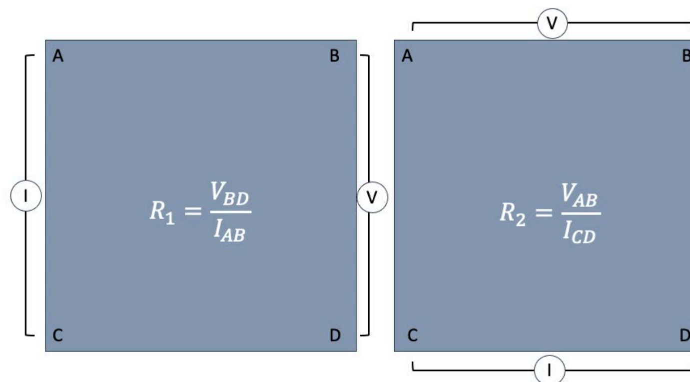

Figure B1 A schematic representation of how R_1 and R_2 are measured on a thin film to calculate ρ_{VDP}. The respective equations to measure R_1 and R_2 are included inside of each configuration [17].

Once *R* v *T* is measured on the PPMS, Equation B1 is applied across the *T* sweep so that the residual resistivity ratio, RRR, can be calculated as,

$$RRR = \frac{\rho_{300K}}{\rho_{5K}} \tag{B2}$$

where ρ_{300K} is the measured vdP resistivity at 300K and ρ_{5K} is the measured vdP resistivity at 5K [19]. This ratio is used to quantify the change in ρ over a range in temperature so that it can be quickly compared to other thin films. Most importantly it captures the quality of a film.

For R v T taken at two different fields, the %MR can be calculated

$$MR(\%) = 100\% * \frac{(\rho_{9T} - \rho_{0T})}{\rho_{0T}} \tag{B3}$$

where ρ_{9T} is the resistivity calculated at each T at 9T and ρ_{0T} is the resistivity calculated at each T at 0T [10]. A 9T field is not necessary for this calculation, and can be substitute with any higher field, but 9T was used for this experiment. The peak typically occurs near T_C. Using MR to determine T_C is not a rigorous analysis because differences arise due to electron transport contributions from the substrate, in the case of this experiment, LSAT [10]. However, the closeness of the peak in %MR to T_C can provide insight into the quality of the film.

Another analysis technique includes looking at the dρ/dT at 0T of the films to see where the maximum change in ρ occurs. This often aligns with the peak in MR, near T_C. This can be seen for the LSMO film in Figure B2(a). This can be compared to the dρ/dT of the LSMO nanowire, seen in Figure B2(b). Similarity in the peak suggests a successful fabrication as discussed before.

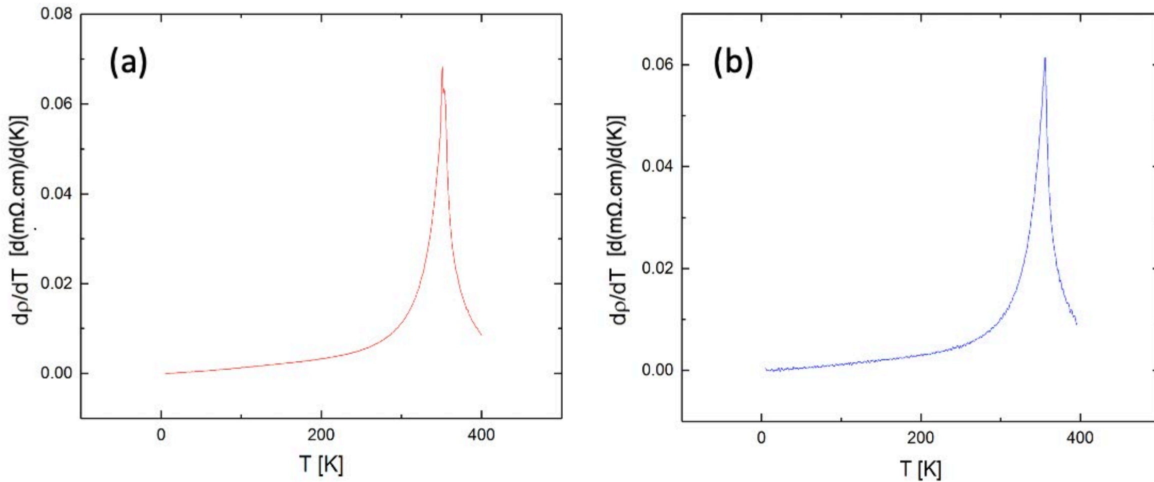

Figure B2 The dρ/dT for (a) the 17.7 nm LSMO film with a peak at 351.06 K, and (b) the LSMO nanowire with peaks at 356.09 K.